Memoirs of the Faculty of Science, Kyoto University, Series of Physics, Astrophysics, Geophysics and Chemistry, Vol. XXXII, No. 1. Article 4, 1967.

MODELS OF THE TRANSITION REGION BETWEEN CHROMOSPHERE AND CORONA

BY

Susumu TOMINAGA

Kwasan Observatory, University of Kyoto

(*Rdeceive July 15, 1967*)

ABSTRACT

In order to obtain a piece of information about Ne and T distributions in the transition region between the chromosphere and corona, observations of *UV* resonance lines are connected with those of radio emission in cm and dm ranges. Models of the transition region are computed for three possible values of the coronal density assuming hydrostatic equilibrium. The models show so steep temperature and density gradients that the *UV* lines of intermediate ions are produced in a very thin regions. The models are not inconsistent with observations of the *UV* bound-free emission and visible continuum in the flash spectrum. It may be inferred from the models that interspicular regions consist of coronal matter with $T\sim10^6$ and $Ne\sim10^9$.

1. Introduction

It is one of the controversial problems in solar physics how varying the physical conditions with height from the low chromosphere ($T<10^4$) to the corona ($T\sim10^6$). Since the structure of the transition region between the chromosphere and corona must be closely connected with the mode of energy transport in the outer solar atmosphere, it is much interesting to know the density and temperature distributions with height through the region.

Many models of the transition region are proposed from different kinds of foundation. Models based on rather theoretical considerations are proposed by SCHATZMAN [1], WOOLLEY and ALLEN [2], and OSTER [3]. A number of approaches based on observed data are made by KOECKELENBERGH [4], PIDDINGTON [5], HAGEN [6] and COATES [7] (the radio observations), by POTTASCH [8] (the observed Ne distribution) and by IVANOV-KHOLODNYI and NIKOLSKII [9], [10] and KOYAMA [11] (the *UV* observation).

In this paper, observations of the *UV* and radio emissions will be analyzed to derive a piece of information about the density and temperature distributions. Using this information, models will be computed under a working assumption of hydrostatic equilibrium. The plausibility of the working models will be discussed referring to the observations of the *UV* bound-free emissions and the visible continuum in the flash spectrum. The models will lead to a picture about the structure of the chromosphere and the innermost corona.

2. Informations about the Ne and T distributions from the UV and Radio Emission

We have the following observational data which may originate in the transition region between the chromosphere and corona: (i) *UV* emission lines, (ii) radio emission in cm and dm ranges, (iii) *UV* continuous emission, (iv) visible continuum in the flash spectrum, and (v) coronal forbidden lines. Of these we shall exclude from our discussion the coronal forbidden lines because it is essentially of coronal origin. We look for a fundamental quantity derived from the observations of (i) and (ii).

(a) *UV* emission lines.

In the analysis of *UV* resonance lines, POTTASCH [12] derived the quantity Q, defined by

$$Q \equiv \frac{N(O)}{N(H)} \int_R N_e^2 dh \,, \tag{1}$$

from the observed intensities of the emission lines. Here $N(O)$, $N(H)$ and N_e are the density of oxygen, hydrogen and electron, respectively, and the integration is limited to the region of formation of the particular observed line.

If we assume the height h above the solar limb and N_e to be one-valued functions of the electron temperature T, we have

$$Q = \frac{N(O)}{N(H)} \int_{T_L}^{T_U} N_e^2 \frac{dh}{dT} dT = A(T_U) - A(T_L) \,, \tag{2}$$

where T_U and T_L are the upper and lower limits of the temperature range assumed by POTTASCH, where the greater part of emission of the relevant line originates from, and $A(T)$ is a function defined by

$$A(T) \equiv \frac{N(O)}{N(H)} \int N_e^2 \frac{dh}{dT} dT \,. \tag{3}$$

By means of the mean value theorem of derivative, we have

$$\left[N_e^2 \frac{dh}{dT} \right]_{T=T_m} = \frac{N(H)}{N(O)} \left[\frac{dA(T)}{dT} \right]_{T=T_m} = \frac{N(H)}{N(O)} \frac{Q}{T_U - T_L} \,, \tag{4}$$

where T_m is a temperature in the range $T_L \leq T \leq T_U$, which may be close to $T_{\max}$ defined by POTTASCH which is the temperature corresponding to the maximum emission, excepting the density factor, of the particular line.

The quantity $\log \left[N_e^2 \frac{dh}{dT} \right]_{T_m}$ is plotted against $\log T$ in Fig. 1, using the data of Q, T_U and T_L, and $N(O)/N(H) = 7 \times 10^{-4}$ determined by POTTASCH. The temperature range and $T_{\max}$ are shown by a bar and a dot, respectively. A smooth curve (the full line) is drawn attaching much weight to the plots of the *O* and *Si* lines, according to the discussion of POTTASCH. This curve represents the quantity

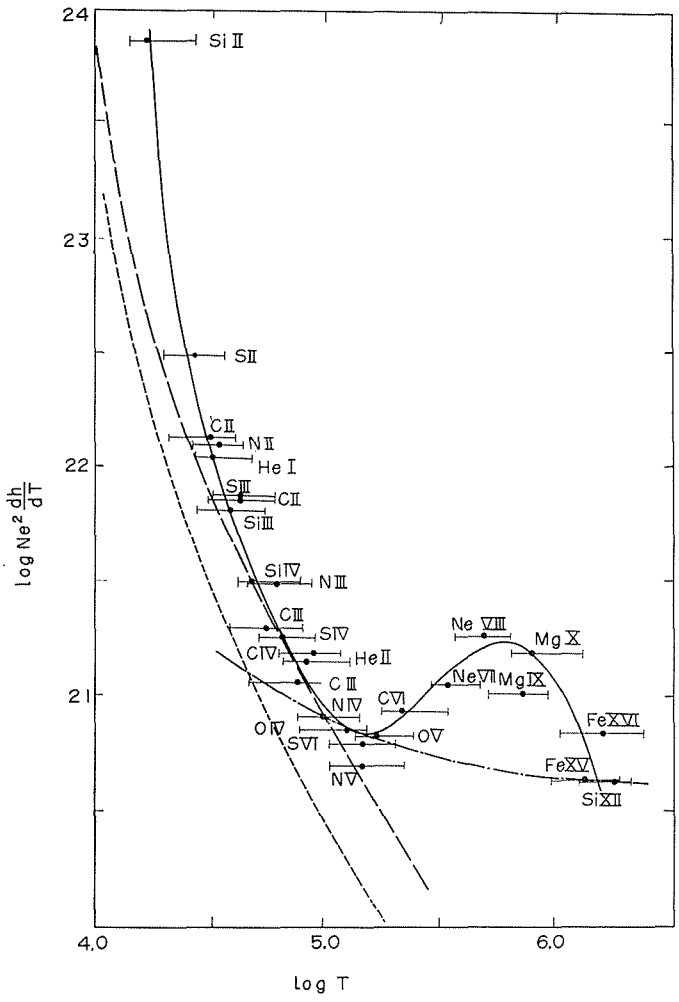

Fig. 1. Comparison between the *UV* and radio emission.

$\left[N_e^2 \frac{dh}{dT} \right]_{UV}$ as a function of T, which is the information about the N_e and T distributions that can be derived from the present *UV* observations.

(b) Radio Emission in cm and dm ranges.

The brightness temperature $T_b(\nu)$ at the disk center in the frequency ν is connected to the local electron temperature $T(\tau_\nu)$ by

$$T_b(\nu) = \int_0^\infty T(\tau_\nu) e^{-\tau_\nu} d\tau_\nu , \qquad (5)$$

where the optical depth τ_ν is defined by

$$\tau_\nu = \int_h^\infty k_\nu dh . \qquad (6)$$

The absorption coefficient k_ν may be expressed by

$$k_\nu = \frac{\zeta N_e^2}{\nu^2 T^{3/2}}, \tag{7}$$

where ζ is a slowly varying functions of N_e, T and ν. Following MORIYAMA [13], we adopt $\zeta=0.14$ in our model computations. We introduce a variable z (cf. PIDDINGTON [5]),

$$z = \int_h^\infty \frac{N_e^2}{T^{3/2}} dh, \tag{8}$$

then we have

$$T_b(\nu) = \frac{1}{\nu^2} \int_0^\infty T(z) e^{-(z/\nu^2)} dz. \tag{9}$$

Since T is a function of z, the right hand side of eq. (9) is the Laplace transform of T with $1/\nu^2$ as the transform variable. Then $T(z)$ will be found if we have an empirical expression of $T_b(\nu)$. PIDDINGTON [14] first found $T_b(\nu)$ at sunspot minimum to be well approximated by

$$T_b(\nu) = a+b\nu^{-1}+c\nu^{-2}, \tag{10}$$

where a, b and c are constants found from the experimental data. From eqs. (9) and (10) the temperature distribution in term of z is given by

$$T(z) = a+\frac{b}{\sqrt{\pi z}}+c\delta(z), \tag{11}$$

where $\delta(z)$ is a discontinuous function, large near the origin and zero elsewhere. PIDDINGTON [5] pointed out that $c\nu^{-2}$ in eq. (10) is a finite contribution to the total emission from a region having negligible optical depth and high temperature, which may be identified with the corona. For the range of higher frequencies where the term $c\nu^{-2}$ may be considerably smaller than the first and second terms of eq. (10), the temperature distribution can be expressed by

$$T(z) = a+\frac{b}{\sqrt{\pi z}}. \tag{12}$$

Then we have from eqs. (8) and (12)

$$N_e^2 \frac{dh}{dT} = -\frac{T^{3/2}}{\zeta} \frac{dz}{dT} = \frac{2b^2}{\pi\zeta} \frac{T^{3/2}}{(T-a)^3}. \tag{13}$$

It is interesting that the quantity $\left[N_e^2 \frac{dh}{dT} \right]_{\text{rad}}$ derived from the radio data has a universal functional form $\propto T^{-3/2}$ for $T \gg a$. This quantity $N_e^2 \frac{dh}{dT}$ as a function of T has also been obtained from the UV emission lines. This comes from the fact

that both the *UV* emission lines and the radio emission originate in twoparticle collision processes.

3. Comparison between the UV and Radio Data.

If the constants a and b in eq. (10) are found from the radio data, we can compare the intensities of *UV* emission lines with those of radio emission through the quantity $N_e^2\frac{dh}{dT}$ which can be regarded as a measure of both the intensities. We should bear in mind here that the validity of the expression (13) is ensured under the conditions that the central brightness temperatures are well approximated in the form of eq. (10) and that the coronal contribution $c\nu^{-2}$ is considerably smaller than others in the frequency range in question. It is the case, as shown by MORIYAMA [13], in the range $\nu>1000$ Mc/s for the quiet sun in the sunspot minimum condition, but in the sunspot maximum phase the coronal contribution becomes greater than others in $\nu<3000$ Mc/s.

In the cm and dm ranges, observed radio emission consists of the basic component (*B*-component) and the slowly varying component (*S*-component). It is well known that the *S*-component originates in regions of high electron temperatures ($T\sim10^{6\circ}$K) and high densities over sunspot groups and plages. Therefore we should exclude the *S*-component in the comparison between the radio emission and the *UV* lines originating in the temperature ranges $T\lesssim 10^{5\circ}$K.

On the other hand the rocket observations give the *UV* emission integrated over the whole atmosphere. Hence the observed *UV* emission must be composed of both contributions from the quiet (dark) and the active (bright) regions, although we could not reliably estimate the intensity ratio and the area fraction of both regions. In fact we have observed evidence [15], [16] that *X*-ray and *Ly-α* line images of the sun show the bright active regions over the quiet background, which reveal a close identification with the *Ca K* spectroheliogram. Therefore the *B*-component of radio emission may correspond to the *UV* emission expected from the hypothetical sun only with the quiet region.

The results of POTTASCH, also our $\left[\log N_e^2\frac{dh}{dT}\right]_{UV}$-curve in Fig. 1, are based on the observations [17], [18], [19] of the rocket flights on April 19 and August 23, 1960, and August 23, 1961. The apparent temperatures T_a of the *B*-component on the days of the flights are computed from the data for four frequencies estimated by TANAKA [20], [21], which are shown in Table 1. We converted the apparent temperatures to the central brightness temperatures T_b (Table 2), using the values of

Table 1. The apparent temperatures of the *B*-component.

Date of flight	T_a			
	9400 Mc/s	3750 Mc/s	2000 Mc/s	1000 Mc/s
Apr. 19, 1960	1.4×10^4	3.7×10^4	9.3×10^4	33×10^4
Aug. 23, 1960	1.4	3.4	8.1	26
Aug. 23, 1961	1.3×10^4	2.8×10^4	6.0×10^4	18×10^4

T_b/T_a given by ALLEN [22]. We determined the constants a, b and c from the brightness temperatures of 9400, 3750 and 2000 Mc/s, which are shown in Table 2 including the values for the B-component in the sunspot maximum and minimum conditions determined by KAKINUMA [23] and by MORIYAMA [13], respectively.

Table 2. The central brightness temperatures of the B-component, the constants a, b and c, and $T_{b,0}$. $T_{b,0}$ is the critical brightness temperature over which the coronal contribution $c\nu^{-2}$ exceeds others.

Date of flight	T_b				a	b	c	$T_{b,0}$
	9400Mc/s	3750Mc/s	2000Mc/s	1000Mc/s				
Apr. 19, 1960	1.1×10^4	2.7×10^4	6.4×10^4	23×10^4	5300	4×10^{13}	1.5×10^{23}	4×10^4
Aug. 23, 1960	1.1	2.5	5.6	19	5600	3.9	1.2	4.5
Aug. 23, 1961	1.1×10^4	2.1×10^4	4.1×10^4	13×10^4	5700	3.9	0.65	7.0
Sunspot maximum					5000	4.5	1.83	3.5
Sunspot minimum					7000	4×10^{13}	0.3×10^{23}	9×10^4

Because the constants a and b remain practically unchanged with the solar cycle as seen in the table, we adopt $a=7000$ and $b=4\times10^{13}$ in the following discussion as the representive values for the days of the three flights. They may be the most reliable values of a and b, because the B-component is well defined in the sunspot minimum conditions. The curve $\log\left[N_e^2\frac{dh}{dT}\right]_{\text{rad}}$ using these values of a and b is shown in Fig. 1 (the dotted line). Meanwhile we see from Table 2 that the constant c changes on a large range with the solar activity. When c has a large value, the validity of eq. (18) is considerably restricted in a range of lower temperatures than in the sunspot minimum. The table contains the critical brightness temperatures $T_{b,0}$ over which the coronal contribution $c\nu^{-2}$ to the brightness temperature beeomes greater than others. By means of the quantity $N_e^2\frac{dh}{dT}$, strictly speaking, we cannot compare the UV intensities with the radio data of the three flights.

(a) The temperature range $1\times10^4\lesssim T\lesssim1\times10^5$.

In the range $T\lesssim4\times10^4$ we can make use of both the curves of $\log N_e^2\frac{dh}{dT}$ in order to compare the UV intensities with the radio data. Fig. 1 exhibits that the UV intensities are stronger over a factor of 3 in this temperature range than expected from the radio data. For instance the disparity in the temperature range of SiII is over an order of magnitude. It should be noted here that the abundance ratios of N, C, S and Si to hydrogen determined by POTTASCH are higher by a factor 2 to 6 than those found by GOLDBERG, MÜLLER and ALLER [24] in the photosphere analysis, although $N(O)/N(H)$ is in good agreement with each other. If one use the latter, the disparity between both the curves will amount to about an order of magnitude even at $T=4\times10^4$.

In order to eliminate this discrepancy between the UV and radio intensities, SUEMOTO and MORIYAMA [25] proposed a chromospheric model in which these two

radiations come only from restricted areas scattered over the whole disk covering about 10% of it which are identified to the spicular structure by them.

The discrepancy may be caused by the following three reasons in addition to the non-uniformity of the emitting region assumed by SUEMOTO and MORIYAMA. First, the strengthening of the lines of low ions, like *Si*II, may be attributed to the chromospheric emission as will be shown latter. Second, the intensities of *UV* lines may be strengthened by the contribution from the bright active regions on the solar disk. The recent *UV* observation [26] referring to the center of the quiet sun shows that there are some differences between the intensities of the quiet sun and the whole sun including active regions. Finally, there might be some systematic errors in the physical constants, especially *f*-values, used in the *UV* analysis. The ALLEN's [27] data of *f*-values used by SUEMOTO and MORIYAMA are lower by about an order of magnitude than those adopted by POTTASCH. Therefore we believe that it is difficult at the present stage of *UV* observations to decide whether the discrepancy should be attributed only to the non-uniform character of the emitting regions or not. Then we assume that the difference of factor 3 at $T\sim 4\times 10^4$ between both the curves in Fig. 1 is caused by the contribution from the bright active region and that the quantity $N_e^2\frac{dh}{dT}$ in the temperature range $4\times 10^4 \lesssim T \lesssim 1\times 10^5$ for the average atmosphere of the quiet and active regions is given by the *UV* data (the full line in Fig. 1), which may be well represented by eq. (18) with $a=7000$ and $b=6.8\times 10^{13}$ (the dashed line in Fig. 1).

As seen in the figure, the *UV* curve still deviates from the dashed line in the temperature range $T<4\times 10^4$. This may be caused by the excess emission of low ions originating in the chromospheric region. We consider *Si*II as an example. According to the *UV* observations [18], the ionizing radiation temperatures of *Si*I and *Si*II are about 5300° and 7200° near their thresholds, respectively. This implies that *Si*II is the most abundant ion of silicon in the atmospheric region where the electron temperature is lower than about 20,000° at which the collisional ionization of *Si*II sets in. Therefore the emitting region of *Si*II should extend over a lower temperature range than that given by POTTASCH ($14{,}000° \lesssim T \lesssim 27{,}000°$) who assumed only the collisional process for ionization.

Although it is difficult to predict the chromospheric emission with accuracy because of little knowledge about the structure, especially the temperature distribution, of the chromosphere, we may estimate the magnitude of the chromospheric emission of *Si*II as follows. Following the analysis of POTTASCH [12], we express the energy flux E measured at the earth's distance by the form

$$E = 3.0\times 10^{-20} P\left(\frac{W}{kT}\right) f_{1u} \int_{h_L}^{\infty} 10^{-5040 W/T} T^{-1/2} Ne N(Si\,\mathrm{II})\, dh\,, \tag{14}$$

where $P\left(\frac{W}{kT}\right)$=a correction factor for the excitation cross section,

f_{1u} =the absorption oscillator strength,

W =the excitation energy in eV,

$N(Si\,\mathrm{II})$=the density of *Si*II ion.

Here the integration should be confined within the region where the diffusion length

$\sqrt{3\lambda}\tau_1 \simeq 1$ for the *SiII* line. The scattering parameter λ may be expressed by [28]

$$\lambda \cong \frac{C_{u1}}{A_{u1}} = 20.60\, \lambda_{\mathrm{cm}}^2 N_e T^{-1/2} P\left(\frac{W}{kT}\right), \tag{15}$$

and the optical depth in the line is given by

$$\tau_1 = \int_{h_L}^{\infty} \alpha N(SiII)\, dh\,, \tag{16}$$

where C_{u1} =the collisional de-excitation rate,
A_{u1} =the spontaneous transition probability,
λ_{cm} =the wave length of the line in cm,
α =the absorption coeffieient at the line center.

If we assume $T=10{,}000°$, $N_e=10^{11}$ and the turbulent velosity $\xi_t=10$ km/sec through the emitting region of *Si*II, we have the following numerical values;

$$\lambda = 2.45\times 10^{-5}, \quad \tau_1 = 117, \quad \text{and} \quad \int_{h_L}^{\infty} N(SiII)\, dh = 4.00\times 10^{14}\,, \tag{17}$$

and from eq. (14) $E=0.95$. This value is in good agreement with the observed value, $E_{SiII}=0.60$, inspite of our rough approximation. Thus the emission of low ions which are most abundant in the chromosphere, like *Si*II, may originate mainly in the chromospheric region of $T\sim 10^4$. Therefore the discrepancy between the *UV* and the dashed curves in Fig. 1 in the temperature range $T<4\times 10^4$ should be attributed to the emission from the chromosphere. Hence we will adopt eq. (13) with $a=7000$ and $b=6.8\times 10^{13}$ (the dashed line in Fig. 1) as the information about the N_e and T distributions in the temperature range $1\times 10^4 \lesssim T \lesssim 1\times 10^5$. The expression (13) should not be applied to much lower temperatures, because some error in the value of a would seriously affect the resultant value of $N_e^2 \frac{dh}{dT}$ in such temperatures.

(b) The high temperature range $T \gtrsim 1\times 10^5$.

As mentioned already, the expression (13) is invalid for higher temperatures where the largest percentage of the radio flux comes from the hot corona. It seems to be the case for $T \gtrsim 1\times 10^5$ as seen in FIG. 1. Hence we should accept the *UV* curve for this high temperature range.

It is of interest that the *UV* curve shows a maximum around $T\sim 6\times 10^5$. In their analysis of the *UV* emission lines, IVANOV-KHOLODNYI and NIKOLSKII [10] found a similar broad maximum in their curve of the "generalized emission measure" $\Delta\varphi \equiv \int_R N_e^2 T^{-3/2} dh$. Using the coronal model of VAN DE HULST [22], they confirmed that the maximum should be attributed to the contribution of the corona to $\varphi\Delta$. We can also estimated the coronal contribution to our quantity $N_e^2 \frac{dh}{dT}$ using the constant c determined from the radio data. From Table 2 we adopt $c=1\times 10^{23}$ as an average of the three flights. Since $c\nu^{-2}$ is the contribution to the central brightness temperature from the corona having negligible optical depth, the constant c can be expressed by

$$c \cong \int_{h_c}^{\infty} \frac{\zeta N_e^2}{T^{3/2}} dh \,, \tag{18}$$

where h_c is the height at the coronal base. Assuming $T=10^6$ °K, $\Delta T \equiv T_U - T_L = 4\times 10^5$ and $\zeta = 0.20$, we have

$$N_e^2 \frac{dh}{dT} = \int_R N_e^2 dh/\Delta T \simeq \int_{h_c}^{\infty} N_e^2 dh/\Delta T \cong cT^{1/2}/\zeta \Delta T = 1.3\times 10^{21}, \tag{19}$$

which corresponds just to the maximum value of $\left[N_e^2 \frac{dh}{dT} \right]_{UV}$ in the order of magnitude. Thus we also confirm that the maximum in our *UV* curve is due to the contribution of the corona.

Since the transition region itself does not have any appreciable contribution to $N_e^2 \frac{dh}{dT}$ in $T > 1\times 10^5$, it is very difficult to estimate the magnitude of the quantity in the transition region. But it may be the best way of interpolate between $T=1\times 10^5$ and 1.6×10^6, making much account of the point of *Si*XII. The reasons are that the intensity of *Si*XII may not be much affected by the outer corona, because the value of $T_{\max}=1.6\times 10^6$ for *Si*XII is more reliable than that of *Fe*XVI ($T_{\max}=1.6\times 10^6$), because the points of silicon ions extend over the widest temperature range. Then we have an empirical expression for the range $1\times 10^5 \lesssim T \lesssim 1.6\times 10^6$,

$$N_e^2 \frac{dh}{dT} = \alpha\left(1+\frac{\beta}{T}\right), \tag{20}$$

where $\alpha = 4.1\times 10^{20}$ and $\beta = 1.0\times 10^5$. The curve (20) is shown by the dash and dotted line in FIG. 1.

4. Models based on the Assumption of Hydrostatic Equilibrium

We summarized the information about the *Ne* and *T* distributions which are obtained from the *UV* and radio data:

$$N_e^2 \frac{dh}{dT} = \frac{2b^2}{\pi\zeta} \frac{T^{3/2}}{(T-a)^3}, \qquad \text{for } 1\times 10^4 \lesssim T \lesssim 1\times 10^5, \tag{21}$$

and

$$N_e^2 \frac{dh}{dT} = \alpha\left(1+\frac{\beta}{T}\right), \qquad \text{for } 1\times 10^5 \lesssim T \lesssim 1.6\times 10^6, \tag{22}$$

where we have taken $a=7000$, $b=6.8\times 10^{13}$, $\zeta=0.14$, $\alpha=4.1\times 10^{20}$ and $\beta=1.0\times 10^5$. These expressions corresopnd to an average atmosphere of the quiet and active regions. Ivanov-Kholodnyi and Nikolskii [9], [10] and Koyama [11] constructed the models of the quiet and active regions, assuming the ratios of the area and brightness between both the regions. However there are observationally very few and uncertain estimates of the ratios for the *UV* lines. Moreover the ratios would be a function of *T*, as inferred from the solar images of *Ca*II, *Ly*-α and *X*-ray. Therefore

we will compute models of the *average* atmosphere using eqs. (21) and (22) as a first approximation.

As mentioned by POTTASCH [12], these expressions would be the maximum information that can be derived from the *UV* and radio observations of the total radiation integrated over the whole atmosphere. But when one attempts to determine N_e and T as a function of h, one must have any other source of the information about the N_e and T distributions. Various kinds of information have been adopted in the previous computations of the models.

PIDDINGTON [5], IVANOV-KHOLODNYI and NIKOLSKII [9], [10] and KOYAMA [11] made use of the quantity $N_e^2T^{-3/2}$ as a function of h, which was derived from the flash spectrum in the eclipse. For the high chromosphere where the flash data do not provide this quantity, they extrapolated to the value of $N_e^2T^{-3/2}$ corresponding to the corona. The extrapolation seems to be very uncertain. Furthermore it is extremely doubtful whether the flash data reflect the real distribution of the quantity $N_e^2T^{-3/2}$ with height. The observed intensity in the flash spectrum is composed of the emission integrated along a line of sight which is cutting across through spicular and interspicular regions even in lower heights, say $h=1500$ km. Since there are certain evidences that interspicular regions have rather lower densities and higher temperatures over an order of magnitude than those in spicules (cf. [28]), the latter may contribute to the observed value of $N_e^2T^{-3/2}$ two or three orders of magnitude more than interspicular regions. Therefore we can say that the observed distribution of $N_e^2T^{-3/2}$ does not reflect the real one, but rather the height distribution of the volume fraction of spicules in line of sight. In fact HIEI [31] found that the number distribution of spicules with height above $h=3000$ km may explain the observed emission gradients of the chromospheric lines. Thus we conclude that the acceptance of the quantity $N_e^2T^{-3/2}$ as a second piece of information should lead to unreliable models of the transition region.

POTTASCH [8] combined the observed density distribution with the assumption of hydrostatic equilibrium to compute the temperature distribution from the chromosphere to the outer corona. For lower heights he used the N_e distribution derived from the observation of the continuum at λ 4700 at the 1952 eclipse [32]. Since the continuous emission of the flash spectrum will also be affected by the spicular structure in the chromosphere, the model of POTTASCH is very uncertain in lower height.

There are several pieces of information about the N_e and T distributions obtained from rather theoretical consideration. WOOLLEY and ALLEN [2] assumed that the temperature is governed only by radial thermal conduction and by radiation loss. HAGEN [6] and COATES [7] performed their computations of the N_e and T distributions under the assumption of equality of pressure between the spicular and interspicular regions. SCHATZMAN [1], KOECKLENBERGH [4], OSTER [3] and POTTASCH [8] assumed hydrostatic equilibrium throughout the chromosphere and the corona. All of these assumptions are not perfectly justified by observations. The analysis of the continuous spectrum taken at the eclipses [31], [33] show that the lower chromosphere is approximately in hydrostatic equilibrium. On the other hand the density gradient in the inner corona is conformable to the same assumption [30]. Even if it is the case, we could not conclude that this assumption should be quite proper in the transition region, because the velosity fields suggested from spicule observations must bring on any departure from hydrostatic equilibrium. However the general aspect of the

transition region may be close to that of the atmosphere in hydrostatic equilibrium, except that one cannot assume a spherical symmetric atmosphere. Then we will compute the N_e and T distributions on the working assumption of hydrostatic equilibrium. The plausibility of the models derived in this way will be discussed referring to the observations of the *UV* bound-free emission and the visible continuum at λ 4700.

Since the turbulent pressure (say, for the turbulent velosity $\xi_t=10$ km/sec) is smaller than the thermal pressure for high temperatures, the equation of hydrostatic equilibrium may be written

$$\frac{d(N_eT)}{dh} = -KN_e \tag{23}$$

where $K = \dfrac{\mu m_H g}{k}$

μ = the mean molecular weight,
m_H = the mass of the hydrogen atom,
g = the surface gravity of the sun,
κ = Boltzman constant,

and we assume $\mu=0.69$ throughout the atmosphere. This expression will not be valid in the range $T \lesssim 2\times10^4$ where hydrogen atoms are not fully ionized and the electron density is not proportional to the total density. For convenience, however, we compute our models with eq. (23) down to $T=1\times10^4$, and so our models are not satisfactorily certain for the temperature range between 1×10^4 and 2×10^4°K.

For $1\times10^5 \lesssim T \lesssim 1.6\times10^6$ we solve the system of eqs. (22) and (23) with the boundary conditions

$$N_eT = (N_eT)_{\rm cor} \quad \text{and} \quad h = h_{\rm cor} \quad \text{at} \quad T = T_{\rm cor} = 1.6\times10^6, \tag{24}$$

where the subscript "cor" refers to the atmospheric region of $T=1.6\times10^6$. The solutions are

$$(N_eT)^2 = (N_eT)^2_{\rm cor} + \alpha K(T_{\rm cor}-T)(T_{\rm cor}+T+2\beta)\,, \tag{25}$$

and

$$h_{\rm cor}-h = \frac{1}{K}\left\{\frac{\sqrt{r}}{2}\ln\frac{\sqrt{r}+(T_{\rm cor}+\beta)}{\sqrt{r}-(T_{\rm cor}+\beta)}\cdot\frac{\sqrt{r}-(T+\beta)}{\sqrt{r}+(T+\beta)} - \frac{\beta}{2}\ln\frac{r-(T+\beta)^2}{r-(T_{\rm cor}+\beta)^2} - (T_{\rm cor}-T)\right\}, \tag{26}$$

where

$$r \equiv \frac{(N_eT)^2_{\rm cor}}{\alpha K} + (T_{\rm cor}+\beta)^2\,. \tag{27}$$

For $T \lesssim 1\times10^5$, if the boundary conditions are set

$$(N_eT) = (N_eT)_0 \quad \text{and} \quad h = h_0 \quad \text{at} \quad T = T_0 \equiv 1\times10^5\,, \tag{28}$$

we have from eqs. (21) and (23)

$$(N_eT)^2 = (N_eT)_0^2 + \frac{4Kb^2}{\pi\zeta} G(T)\,, \tag{29}$$

where

$$G(T) \equiv 2(\sqrt{T_0} - \sqrt{T}) + \frac{15\sqrt{a}}{8} \ln \frac{\sqrt{T_0} - \sqrt{a}}{\sqrt{T_0} + \sqrt{a}} \cdot \frac{\sqrt{T} + \sqrt{a}}{\sqrt{T} - \sqrt{a}}$$
$$+ \frac{a}{4} \left\{ \frac{\sqrt{T}(9T - 7a)}{(T-a)^2} - \frac{\sqrt{T_0}(9T_0 - 7a)}{(T_0 - a)^2} \right\}. \tag{30}$$

Here the subscript "o" refers to the atmospheric region of $T = 1 \times 10^5$. The value of $(N_eT)_0$ is given by eq. (25) with $T = 1 \times 10^5$, which is shown in the following table for possible values of $Ne_{\rm cor}$.

$N_{e\,\rm cor}$	1.0×10^8	3.0×10^8	5.0×10^8
$(N_eT)_0$	5.4×10^{14}	7.0×10^{14}	9.5×10^{14}

From eq. (30), on the other hand, we find

$$1.2 \times 10^{14} \geqq \left\{ \frac{4Kb^2}{\pi\zeta} G(T) \right\}^{1/2} \geqq 0\,, \qquad \text{for } 1 \times 10^4 \leqq T \leqq 1 \times 10^5\,, \tag{31}$$

and the middle term decreases rapidly with increasing temperature, so that we can neglect the second term in the right-hand side of eq. (29) with sufficient accuracy for our purpose. It follows that in the temperature range $1 \times 10^4 \leqq T \leqq 1 \times 10^5$ the assumption of hydrostatic equilibrium is approximately equivalent with the assumption of N_eT=constant with T. Thus we solved eq. (21) on the assumption $N_eT = (N_eT)_0$. The solution is

$$h_0 - h = \frac{2b^2}{\pi\zeta (N_eT)_0^2} \left[\frac{2}{3} (T_0^{3/2} - T^{3/2}) + 6a(\sqrt{T_0} - \sqrt{T}) \right.$$
$$+ \frac{a^2}{4} \left\{ \frac{\sqrt{T}(13T - 11a)}{(T-a)^2} - \frac{\sqrt{T_0}(13T_0 - 11a)}{(T_0 - a)^2} \right\}$$
$$\left. + \frac{35a^{3/2}}{8} \ln \frac{\sqrt{T_0} - \sqrt{a}}{\sqrt{T_0} + \sqrt{a}} \cdot \frac{\sqrt{T} + a}{\sqrt{T} - a} \right] \tag{32}$$

For the three possible values of $N_{e,\rm cor}$ in the above table, we compute the N_e and T distributions by means of eqs. (25), (26) and (32). The results are shown in Table 3, 4 and 5 and Fig. 2, 3 and 4. The zero point of the height scale cannot be set in our models. The models of the low chromosphere obtained from the continuum analysis [31], [33] show that the low chromosphere below about h=1000 km may be considered to be a spherically symmetric layer of $T < 10{,}000$°K. Above this layer, we should take account of the distribution between the spicular and the interspicular regions. Since the interspicular regions may have a higher temperature than 10,000°K [28], it may be reasonable to assign the top of the low chromosphere to the temperature region of $T = 1 \times 10^4$ in our models, so that in Fig. 2 and 3 we set up the height h_1 of $T = 1 \times 10^4$ as 1000 km. Thus the height distributions of N_e and

Table 3. Model (a) for $N_{e,\,cor}=1.0\times10^{8}$.

T	$h-h_1$ (cm)	N_e	T	$h-h_1$ (cm)	N_e
1.0×10^{4}	0.00	5.39×10^{10}	5.0	8.35×10^{7}	1.02×10^{9}
2.0	6.01×10^{5}	2.69	6.0	1.41×10^{8}	8.32×10^{8}
3.0	1.11×10^{6}	1.80	7.0	2.24	6.93
4.0	1.38	1.35	8.0	3.40	5.85
5.0	1.63	1.08×10^{10}	9.0×10^{5}	4.97	4.99
6.0	1.89	8.99×10^{9}	1.0×10^{6}	7.10	4.27
7.0	2.15	7.70	1.1	9.98×10^{8}	3.65
8.0	2.42	6.74	1.2	1.40×10^{9}	3.08
9.0×10^{4}	2.69	5.99	1.3	1.95	2.58
1.0×10^{5}	2.97	5.39	1.4	2.77	2.09
2.0	9.31×10^{6}	2.68	1.5	4.07	1.58
3.0	2.16×10^{7}	1.76	1.6×10^{6}	6.71×10^{9}	1.00×10^{8}
4.0	4.48	1.30			

Table 4. Model (b) for $N_{e,\,cor}=3.0\times10^{8}$.

T	$h-h_1$ (cm)	N_e	T	$h-h_1$ (cm)	N_e
1.0×10^{4}	0.00	7.04×10^{10}	5.0	4.73	1.37
2.0	3.52×10^{5}	3.52	6.0	7.95×10^{7}	1.12×10^{9}
3.0	6.50	2.35	7.0	1.24×10^{8}	9.47×10^{8}
4.0	8.06	1.76	8.0	1.84	8.14
5.0	9.56×10^{5}	1.41	9.0×10^{5}	2.65	7.08
6.0	1.11×10^{6}	1.17	1.0×10^{6}	3.68	6.22
7.0	1.26	1.01×10^{10}	1.1	4.99	5.49
8.0	1.42	8.80×10^{9}	1.2	6.66	4.87
9.0×10^{4}	1.58	7.82	1.3	8.76×10^{8}	4.33
1.0×10^{5}	1.74	7.04	1.4	1.14×10^{9}	3.85
2.0	5.44×10^{6}	3.50	1.5	1.48	3.41
3.0	1.32×10^{7}	2.32	1.6×10^{6}	1.90×10^{9}	3.00×10^{8}
4.0	2.27	1.73			

Table 5. Model (c) for $N_{e,\,cor}=5.0\times10^{8}$.

T	$h-h_1$ (cm)	N_e	T	$h-h_1$ (cm)	N_e
1.0×10^{4}	0.00	9.51×10^{10}	5.0	2.57	1.87
2.0	1.93×10^{5}	4.76	6.0	4.28	1.55
3.0	3.57	3.17	7.0	6.61	1.32
4.0	4.42	2.38	8.0	9.68×10^{7}	1.14
5.0	5.14	1.90	9.0×10^{5}	1.37×10^{8}	1.00×10^{9}
6.0	6.06	1.59	1.0×10^{6}	1.88	8.92×10^{8}
7.0	6.90	1.36	1.1	2.51	8.00
8.0	7.76	1.19	1.2	3.28	7.22
9.0×10^{4}	8.65	1.06×10^{10}	1.3	4.23	6.56
1.0×10^{5}	9.53×10^{5}	9.51×10^{9}	1.4	5.35	5.98
2.0	2.68×10^{6}	4.75	1.5	6.69	5.46
3.0	7.47×10^{6}	3.15	1.6×10^{6}	8.29×10^{8}	5.00×10^{8}
4.0	1.40×10^{7}	2.35			

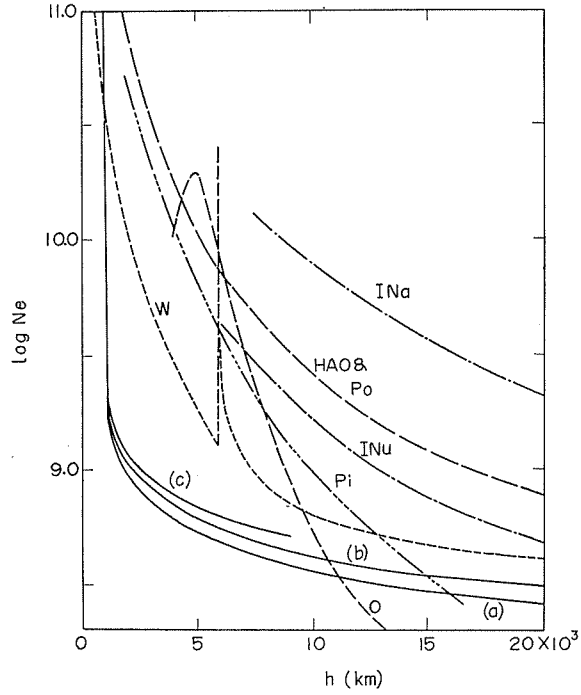

Fig. 2. Distributions of the electron density in the transition region. The full lines: The present models, WA: WOOLLEY and ALLEN [2], O: OSTER [3], Pi: PIDDINGTON [5], HAO & Po: The HAO data [32] and POTTASCH [8], IN: IVANOV-KHOLODNYI and NIKOLSKII [10] (a= active, u=undisturbed regions).

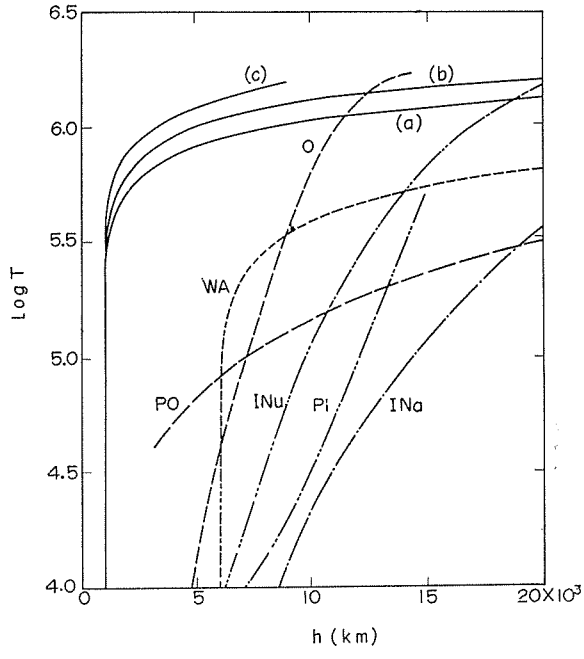

Fig. 3. Distributions of the electron temperature in the transition region. Cf. the legend of FIG. 2.

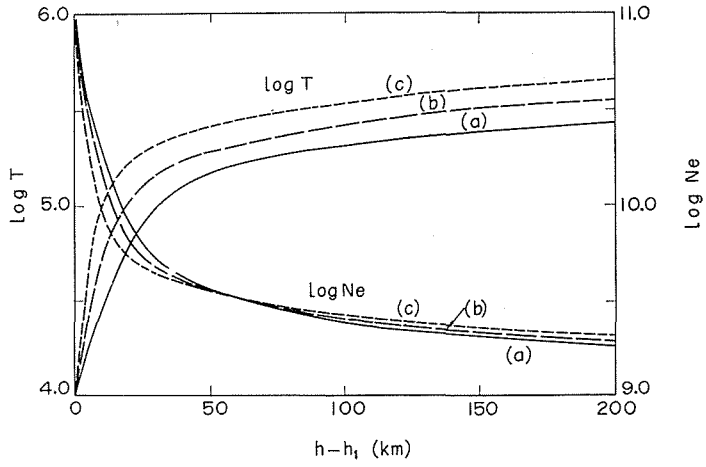

Fig. 4. N_e and T distributions in the boundary region of the present models.

T in our models should correspond to the interspicular medium. In our model computations we assumed the condition N_eT=constant for $1\times10^4 \leqq T \leqq 1\times10^5$, which may approximately hold also in the boundary between the spicular and the interspicular regions. Hence the very steep gradients of the N_e and T distributions shown in Fig. 4 refer to the outer boundary of spicules as well as the top of the low chromosphere.

A sheath-like structure of spicules is proposed by MORIYAMA [13] from the analysis of the 1952 eclipse data, and by SUEMOTO and HIEI [34] from the appearance of the flash spectrum in the 1958 eclipse. It may be inferred also from our models that the individual spicule is surrounded by a very thin transition region in a form of sheath and the interspicular regions consist of coronal matter with $T\sim10^6$ and $N_e\sim10^9$. The transition from $T=1\times10^4$ to 1×10^5 occures in a geometrical thickness of the order of 10 km, thus the possibility of any extend high temperature plateau in the upper chromosphere should be ruled out.

5. Discussion of the Models.

(a) *UV* bound-free emission.

The Lyman continuum of hydrogen is the most well-defined and conspicuous one in the *UV* region. The 504 and 228 continua of *He*I and *He*II are also observed. We compute the photon flux of these continua predicted from our models, to compare with the observations.

The number of recombination to the n-th level per cm^3 per sec is given by

$$F_{kn}d\lambda = \frac{4\pi h^3 c}{(2\pi mk)^{3/2}} \frac{\varpi_n}{B_i} \frac{10^{24}}{\lambda^4} \alpha_n(\lambda) \frac{N_i N_e}{T^{3/2}} e^{-\frac{10^8 hc}{kT}\left(\frac{1}{\lambda}-\frac{1}{\lambda_n}\right)} d\lambda \,, \tag{33}$$

where ϖ_n =the statistical weight of the n-th level,
B_i =the partition function of the ion,

$\alpha_n(\lambda)$=the atomic absorption coefficient at wavelength λ,
N_i =the ion density,
λ_n =the wavelength at the threshold,

and the wavelengths are in units of Å. Thus the photon flux $\phi(\lambda)$ in $d\lambda$=1 Å measured at the earth's distance is expressed in the form

$$\phi(\lambda) = \frac{1}{2}\left(\frac{R_\odot}{AU}\right)^2 \int_{h_L}^{\infty} F_{kn}\,dh = \frac{1}{2}\left(\frac{R_\odot}{AU}\right)^2 \frac{4\pi h^3 c}{(2\pi mk)^{3/2}} \frac{\varpi_n}{B_i} \frac{10^{24}}{\lambda^4}\alpha_n(\lambda)$$
$$\times \int_R \frac{N_i}{N_e}\frac{1}{T^{3/2}} \cdot e^{-\frac{10^8 hc}{kT}\left(\frac{1}{\lambda}-\frac{1}{\lambda_n}\right)}\left[N_e{}^2\frac{dh}{dT}\right]dT, \tag{34}$$

where $R_\odot$ is the solar radius, AU the astronomical unit and the integration should be limited to the atmospheric region through which the diffusion length for the continuum is equal to unity. The photon fluxes at the threshold are numerically given as follows:

for the Lyman continuum, $$\phi(912) = 3.1\times10^{-14}\int_R \frac{N_p}{N_e}\frac{1}{T^{3/2}}\left[N_e{}^2\frac{dh}{dT}\right]dT, \tag{35}$$

for the 504 continuum of *He*I, $$\phi(504) = 9.9\times10^{-14}\int_R \frac{N_{\rm II}}{N_e}\frac{1}{T^{3/2}}\left[N_e{}^2\frac{dh}{dT}\right]dT, \tag{36}$$

for the 228 continuum of *He*II, $$\phi(228) = 2.2\times10^{-12}\int_R \frac{N_{\rm III}}{N_e}\frac{1}{T^{3/2}}\left[N_e{}^2\frac{dh}{dT}\right]dT, \tag{37}$$

where N_p, $N_{\rm II}$ and $N_{\rm III}$ are the density of proton, *He*II and *He*III ions, respectively.

In order to predict the photon flux of the continua, we have to know the density distribution of ions as a function of T. The ionization degree of *H*I, *He*I and *He*II have been computed, assuming that (i) the ionization is caused by both radiative and collisional processes, (ii) the ionization degree is determined by the modified Saha equation,

$$\frac{N_{i+1}N_e}{N_i} = \frac{(2\pi mk)^{3/2}}{h^3}\frac{2B_{i+1}}{B_i}T_r{}^{3/2}e^{-(I/kT_r)}S\sqrt{\frac{T_e}{T_r}}, \tag{38}$$

for the radiation process, and by the ionization formula given by POTTASCH [12] for the collisional process, and (iii) the condition $N_eT=(N_eT)_0$ is valid through the lower temperature range according to our models. A numerical example of the density distributions is shown in Fig. 5 for the following case:

$(N_eT)_0$ $=7.0\times10^{14}$ (i.e., $N_{e,\rm cor}=3.0\times10^8$),
$T_r(912)=6650°$,
$T_r(504)=10{,}900°$,
$T_r(228)=21{,}900°$,
S $=\frac{1}{2}$ and $N(He)/N(H)=0.2$

where T_r is the radiation temperature of the continuum inferred from the *UV* observations [18] and S the dilution factor, then the photon flux can be computed from eqs. (35), (36) and (37), and is shown in Table 6. The integration is performed

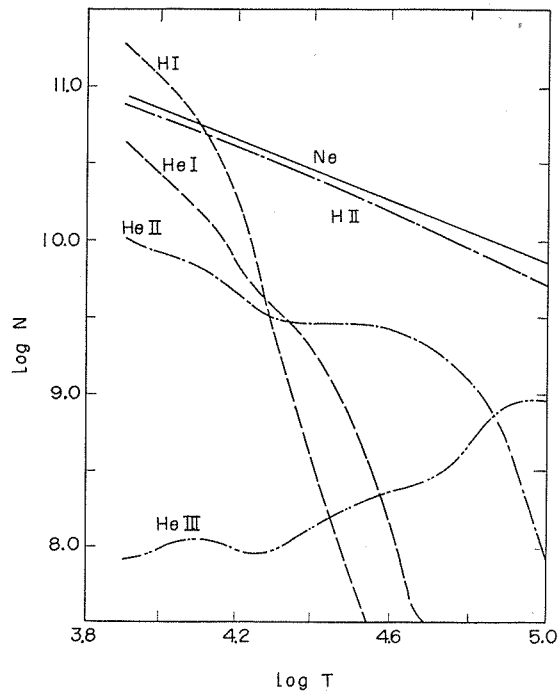

Fig. 5. Density distributions versus the temperature in the case of $N_{e,\,cor}=3.0\times10^{8}$.

Table 6. The photon flux of the bound-free emissions for case of $N_eT=7.0\times10^{14}$, in units of photons/cm^2/sec in $d\lambda=1$ Å.

Observed photon flux	Computed photon flux			Optical depth to the region of $T=1\times10^4$
	log T_L=4.00	log T_L=3.95	log T_L=3.90	
$\phi(912)^{a)}=2.5\times10^8$	3.3×10^7	8.7×10^7	4.3×10^8	0.12
$\phi(504)^{b)}=6.2\times10^7$	1.5×10^7	3.7×10^7	1.8×10^8	0.043
$\phi(228)^{c)}=8.1\times10^7$	5.8×10^6	1.1×10^4	3.8×10^7	0.009

a) The observation [18] of Aug. 23, 1960.
b) The observation [19] of Aug. 23, 1961, assuming the atmospheric optical depth at the altitude of 225 km, $\tau_{225}=0.57$ and the instrumental wavelength bandwidth $\Delta\lambda=2.0$ Å.
c) The observation [18] of Aug. 23, 1960, averaging the emission of lines and continuum between 226 Å and 166 Å.

over the temperature range between T_L given in the table and $T_{cor}=1.6\times10^6$, using the expressions (21) and (22).

If the integration is limited to $T\geqq1\times10^4$, the predicted flux is an order of magnitude smaller than the observed value. This may not mean that our model for $N_{e,\,cor}=3\times10^8$ is contrary to the observations of bound-free emission, because the emitting region must extend to the low temperature region (the chromosphere). As shown in Table 6, the optical thickness of the transition region ($T\gtrsim1\times10^4$) are much smaller than unity, and the major part of the *H*I, *He*I and *He*II continua comes from the chromosphere ($T\lesssim1\times10^4$).

(b) The continuum at λ 4700 at the 1952 eclipse.

The continuum emission at λ 4700 has been analyzed for the flash spectrum taken by HAO expedition [32] at the 1952 eclipse. The analysis of the continuum data [33] suggests that for $h \gtrsim 2000$ km the emission at λ 4700 is almost due to electron scattering. Using the N_e distribution of our models, we compute the total emission at λ 4700 to compare with the observed values. Fig. 6 exhibits the N_e distributions

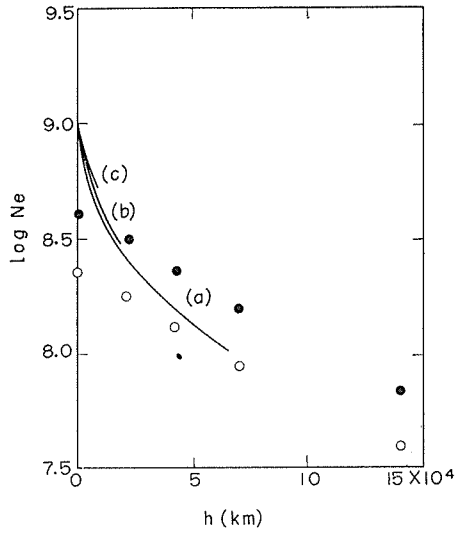

Fig. 6. Comparison of the N_e distributions in the inner corona. The full lines: The present models. The filled and open circle: Coronal models of VAN DE HULST [30].

in our models, together with the coronal models of VAN DE HULST [30]. It seems that the N_e distributions for $N_{e,\,\mathrm{cor}}=3.0\times10^8$ and 1.0×10^8 are smoothly connected with the sunspot maximum and minimum (equator) models, respectrively, taking account that the VAN DE HULST's models close to the sun's limb are based on an extrapolation. Since the atmospheric condition at the 1952 eclipse is close to the minimum phase, we take the transition region model of $N_{e,\,\mathrm{cor}}=1.0\times10^8$ and the coronal model in the sunspot minimum along the equator.

We first compute the total emission which is expected from the VAN DE HULST's coronal models. The surface brightness of the K plus F components tabulated by him is well represented by

$$K+F=\frac{3.55\times10^4}{r^{17}}+\frac{1.91\times10^4}{r^7}+\frac{5.89\times10^2}{r^{2.5}}$$

for the maximum phase, (39)

and

$$K+F=\frac{2.09\times10^4}{r^{17}}+\frac{1.10\times10^4}{r^7}+\frac{5.89\times10^2}{r^{2.5}}$$

for the minimum (equzator) phase, (40)

where $r=(R_\odot+h)/R_\odot$ and $K+F$ is expressed in the unit of 10^{-10} times the average surface brightness of the solar disk. These expressions are applicable in all wavelengths, because the K and F components of the coronal light have a continuous spectrum with nearly the same color as the sun. Then the total emission at λ 4700 (ergs cm^{-1} sec^{-1} in all directions per unit frequency) is given by

$$E_{cor}(h) = 4\pi\bar{I}_\nu(\lambda\,4700)R_\odot\times10^{10}\int_{r(h)}^{\infty}(K+F)dr\,, \tag{41}$$

where $\bar{I}_\nu(\lambda\,4700)$ is the mean intensity of the photospheric radiation at λ 4700 and we adopt $\bar{I}_\nu(\lambda\,4700)=2.28\times10^{-5}$. The curves of $E_{cor}(h)$ for the maximum and the minimum (equator) phases are shown in Fig. 7 by the full lines. Next we must take accounts of the excess of N_e near the limb over the coronal model, which may numerically be represented by

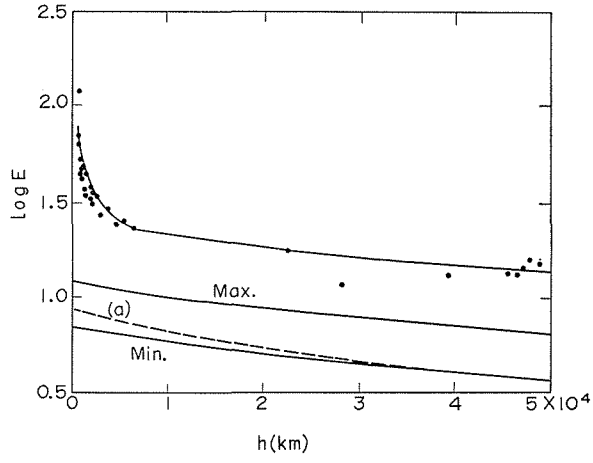

Fig. 7. The total emission at λ 4700. The observed values in the 1952 eclipse [**35**] are denoted by the filled circles with the best fitting curve.

$$\begin{aligned}\Delta N_e &\equiv N_e\ (\text{our model}) - N_e\ (\text{minimum corona})\\ &= 3.24\times10^{9}\exp(-1.45\times10^{-8}h)\\ &\quad +5.73\times10^{8}\exp(-2.95\times10^{-9}h)\\ &\quad +2.69\times10^{8}\exp(-5.76\times10^{-10}h)\,,\end{aligned} \tag{42}$$

for $h\gtrsim2000$ km in the model of $N_{e\,cor}=1.0\times10^{8}$. Thus we can compute the additional emission ΔE due to the excess of N_e. The curve of $\log(E_{cor}+\Delta E)$ is shown by the dotted line in Fig. 7, together with the observed values and the best fitting curve [35]. It is noted that the excess of N_e over the coronal model would introduce only a slight rise of the curve near the limb and that the form and size of $\log E$ for $h\gtrsim$ 10,000 km would be practically determined by the contribution of the corona. Furthermore, there is a remarkable difference in the absolute intensities between the observed and predicted curves in all heights. The highest point of the HAO observation is about 50,000 km ($r=1.07$). The photometric data of VAN DE HULST

should be reliable above this height at least. Nevertheless, $\log E$ at $h\sim 50{,}000$ km differs about 0.5 compared with the minimum corona and about 0.3 even compared with the maximum corona. Hence it seems improbable to ascribe its origin to a difference in physical state of the chromosphere and corona from one eclipse to another, we could not escape from the conclusion that all intensities derived from the HAO 1952 eclipse observations should be reduced by about a factor 2 or 3, as suggested by ATHAY, MENZEL and ORRALL [36].

If the observed values of $\log E$ in Fig. 7 are brought down by about 0.5, we find a good agreement with the predicted curve of the case $N_{e,\,\mathrm{cor}}=1.0\times 10^8$ for $h>5000$ km. The high observed values of $\log E$ below 5000 km may be attributed to the contribution of the chromospheric spicules. Therefore it is not likely that our models are inconsistent with the observation of the λ 4700 continuum.

(c) Comparison with other models.

The quantity $N_e^2\frac{dh}{dT}$ as a function of T (eqs. (21) and (22)) is the fundamental information which is derived from the observations of the radio and *UV* emissions. Any model of the transition region should be conformable with this information. Fig. 8 exhibits the quantity computed from the N_e and T distributions of the typical models proposed by other authors to compare with the curves of eqs. (21) and (22).

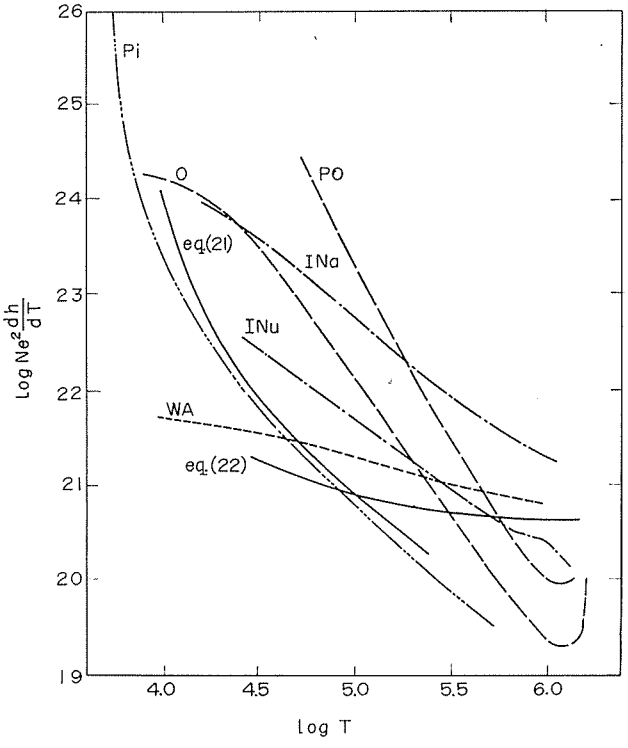

Fig. 8. Comparison of $N_e^2\frac{dh}{dT}$. Cf. the legend of Fig. 2.

The model of WOOLLEY and ALLEN [2] is in reasonable agreement with eq. (22) for $T \gtrsim 10^5$, but the model gives too low values of $N_e^2 \frac{dh}{dT}$ for $T \lesssim 10^5$ to yield sufficient intensities of the *UV* lines of low ions. This may imply that their assumption of heat conduction as the principal energy souree does not hold for the temperature range $T \lesssim 10^5$.

OSTER [3] constructed his models bashing on an arbitrary interpolation of the thermal plus turbulent pressure between the values corresponding to the upper chromosphere and the lower corona. It is seen in Fig. 8 that his Model II shows marked discrepancies in lower and higher temperature ranges, and his simple interpolation of the pressure may lead to unreliable distributions of N_e and T with height. BROOKS and OSTER [37] computed the thermal radio emission on the basis of the OSTER models with the aid of more correct absorption coefficient, and found that the models, in particular Model II, predict the radio emission in the dm range quite accurately. But the agreement with the observations seems not to be so good as stated by them. Taking into account the fact that they compared the computed values with the observed "*radiation temperatures*" which contain the apparent temperatures including the coronal contribution (the term $c\nu^{-2}$ in eq. (15)), it can be said that the OSTER models give an overestimate of the radiation temperature throughout the cm and dm ranges as expected from Fig. 8. In comparison with the observed intensities of *UV* emission lines, ALLER [27] concluded that the Model II of OSTER is in rough agreement with the observations. This may be due to the facts that he adopted the much low *f*-values and that he ignored the chromospheric contribution to the emission of low ions (I and II).

The model of PIDDINGTON [5] gives the curve $N_e^2 \frac{dh}{dT}$ which is in good agreement with eq. (21) for $T \lesssim 10^5$. However he used the height distribution of $N_e^2 T^{-3/2}$ obtained from the flash spectrum. We believe that the observations at the sun's limb do not give the real distributions of any physical quantites, but those influenced by the spicular structure of the chromosphere. PIDDINGTON [5] rejected the models of SCHATZMAN [1] and KOEKELENBERGH [4] based on the assumption of hydrostatic equilibrium, because their models are grossly inconsistent with the flash data. This criticism may also be applied to our models. However, it should be necessary to reanalyze the flash data taking proper account of the spicular structure.

The effect of spicules seems to appear seriously in the model of POTTASCH [8] who adopted the flash data of the N_e distribution and the assumption of hydrostatic equilibrium. It is shown in Fig. 8 that the POTTASCH [8] model should predict too high intensities of the radio and *UV* emission. This discrepancy may not be caused by the assumption of hydrostatic equilibrium, but by the acceptance of the height distribution of N_e obtained from the flash saectrum.

IVANOV-KHOLODNYI and NIKOLSKII [9], [10] also made use of the height distribution of $N_e T^{2-3/2}$ which must not give any real information of the N_e and T distributions as stated above. Furthermore the separation of active and undisturbed regions is based on a quite uncertain estimate of the area and brightness ratios of both regions.

In Figs. 2 and 3 the N_e and T distributions of our models are compared with those of other models. It is characteristic of our models that there occur marked

steep gradients of the N_e and T distributions in the ranges $N_e \gtrsim 10^9$ and $T \lesssim 4\times 10^5$, so that we can find coronal matter of $T\sim 10^6$ in the interspicular regions below $h=$ 5000 km. This is compatible with the observation of ATHAY and ROBERTS [38] that the *Fe*XI line at λ 7892 is measured over a height range $2000 \lesssim h \lesssim 46{,}000$ km in the 1952 eclipse and that the maximum intensity occured below 10,000 km. Our models may account for emission from *Fe*XI at height as low as 5000 km.

7. Conclusion.

The analysis of the *UV* resonance lines and the cm and dm radio emission made possible to compare their intensities with each other through the common quanttiy $N_e^2 \frac{dh}{dT}$ as a function of T (Fig. 1). In comparison with *B*-component of the radio emission, the intensities of the *UV* lines originating in $T\sim 4\times 10^4$ are stronger about a factor of 3 than expected from the radio emission. This discrepancy has been tentatively attributed to the contribution of the bright active regions on the solar disk to the *UV* line emissions.

The information about the N_e and T distributions is expressed in an analytical form (eqs. (21) and (22)), which has simultaneously been solved with the equation of hydrostatic equilibrium. The models imply that the surface of high density medium, i.e. the low chromosphere and the spicules, are covered by a very thin transition region responsible for emission of intermediate ions and radio waves in cm and dm ranges. Thus we may have a picture that the high chromosphere should be identified with the spicules which penetrate into the interspicular regions consisting of coronal matter and are surrounded by a very thin hot sheath.

The author wishes to express his hearty thanks to Prof. S. Miyamoto for his invaluable advice and constant encouragement. Grateful acknowledgement is due to Drs. I. Kawaguchi and M. Kanno for their critical comments and suggestions, and to Dr. S. Saito for his reading the manuscript of this paper. Many thanks are also due to all the staff members of the Kwasan Observatory for their helpful discussion and encouragement.

REFERENCES

1) E. Schatzman, Ann. d'Ap., **12**, 203, 1949.
2) R.v.d.E. Woolley and C.W. Allen, M.N., **110**, 358, 1950.
3) L. Oster, Zs. f. Ap., **40**, 28, 1956.
4) A. Koeckelenbergh, Bull. Acad. Roy. Belgique, **37**, 252, 1951.
5) J.H. Piddington, Ap. J., **119**, 531, 1954.
6) J.P. Hagen, IAU symp. No 41 Radio Astronomy, ed. van de Hulst (Cambridge Univ. Press), p. 263, 1957.
7) R.J. Coates, Ap. J., **128**, 83, 1958.
8) S.R. Pottasch, Ap. J., **131**, 68, 1960.
9) G.S. Ivanov-Kholodnyi and G.M. Nikolskii, Soviet A. J., **38**, 45, 1961.
10) G.S. Ivanov-Kholodnyi and G.M. Nikolskii, Soviet A.J., **39**, 777, 1962.
11) S. Koyama, Publ. A. S. Japan, **15**, 15, 1963.
12) S.R. Pottasch, Ap. J., **137**, 945, 1963.
13) F. Moriyama, Ann. Tokyo Astr. Obs., 2nd ser., **7**, 127, 1961.
14) J.H. Piddington, Proc. Roy. Soc. London, **A, 203**, 417, 1950.

15) T.A. Chubb, H. Friedman, H.W. Kreplin, H.L. Blake and A.E. Unzicker, Mem. Soc. Roy. Sci. Liege, 5th ser., **4**, 235, 1961.
16) J.D. Purcell and R. Tousey, Mem. Soc. Roy. Sci. Liege, 5th ser., **4**, 274, 1961.
17) C.H. Detwiler, D.L. Garrett, J.D. Purcell and R. Tousey, Ann. geophys., **17**, 1961.
18) H.E. Hinteregger, J. Geophys. Res., **66**, 2367, 1o961.
19) L.A. Hall, K.R. Damon and H.E. Hinteregger, 3rd COSPAR symp. Space TResearch III, ed. Priester (Amsterdam: North-Holland), p. 745, 1963.
20) H. Tanaka, Proc. Res. Inst. Atmospherics, Nagoya Uhiv., **11**, 41, 1964.
21) Private communication.
22) C.W. Allen, IAU symp. No 41 Radio Astronomy, ed. van de Hulst (Cambridge Univ. Press), p. 253, 1967.
23) T. Kakinuma, Bull. Res. Inst. Atmospherics, Nagoya Univ., **12**, 15, 1962.
24) L. Goldberg, E.A. Müller and L.H. Aller, Ap. J. Suppl., **5**, No 45, 1960.
25) Z. Suemoto and F. Moriyama, 3rd COSPAR symp. Space Research III, ed. Priester (Amsterdam: North-Holland), p. 806, 1963.
26) L. Goldberg, W.H. Parkinson, E.M. Reevers and R.W. Noyes, A.J., **69**, 140, 1964.
27) C.W. Allen, Mem. Soc. Roy. Sci. Liege, 5th ser., **4**, 241, 1961.
28) H. Zirin and H.D. Dietz, Ap. J., **138**, 664, 1963.
29) H. van Regemorter, Ap. J., **136**, 906, 1962.
30) H.C. van de Hulst, The Sun, ed. Kuiper (Chicago Univ. Press), p. 207, 1953.
31) R.G. Athay, D.H. Menzel, J.-C. Pecker and R.N. Thomas, Ap. J. Suppl., **1**, No 12, 1955.
33) S.R. Pottasch and R.N. Thomas, Ap. J., **132**, 195, 1960.
34) Z. Suemoto and E. Hiei, Publ. A.S. Japan, **14**, 33, 1962.
35) R.N. Thomas and R.G. Athay, Physics of the Solar Chromosphere (New York: Interscience Publisher), p. 36, 1961.
36) R.G. Athay, D.H. Menzel and F.Q. Orrall, Smithsonian Contr. Astrophys., **2**, 35, 1957.
37) C.C. Brooks and L. Oster, Ap. J., **134**, 940, 1961.
38) R.G. Athay and W.O. Roberts, Ap. J., **121**, 231, 1955.